GEOPHYSICAL & ASTROPHYSICAL FLUID DYNAMICS, 2017
VOL. 111, NO. 2, 91–114
http://dx.doi.org/10.1080/03091929.2017.1287909

Taylor & Francis
Taylor & Francis Group

Internal dissipative boundary layers in the cross-equatorial flow of a grounded deep western boundary current

Gordon E. Swaters[a,b]

[a]Department of Mathematical and Statistical Sciences, Applied Mathematics Institute, University of Alberta, Edmonton, Canada; [b]Institute for Geophysical Research, University of Alberta, Edmonton, Canada

ABSTRACT

It is known that dissipative adjustment must occur in the cross-equatorial dynamics of a deep western boundary current (DWBC) that is in planetary-geostrophic balance away from the equator. Theoretical modelling and numerical simulations suggest that the dissipative zones correspond to "small" isolated zonally-elongated regions within the trough and crest of a nonlinear stationary equatorial planetary wave that is formed as the DWBC flows eastward along the equator. An internal frictional boundary layer theory is advanced to describe the leading order structure of the DWBC in the dissipative regions, which asymptotically matches with the large scale inviscid flow characteristics in the equatorial region.

ARTICLE HISTORY
Received 4 July 2016
Accepted 24 January 2017

KEYWORDS
Grounded abyssal ocean currents; deep western boundary currents: cross-equatorial flow; frictional boundary layers

1. Introduction

The deep waters produced in the Labrador and Norwegian/Greenland Seas by atmospheric cooling flow toward the equator as part of the deep western boundary currents (DWBCs) in the Atlantic Ocean. In midlatitudes, away from the equator and on the North American continental slope, these currents correspond to a grounded abyssal flow on a sloping bottom with upslope and down slope incroppings or groundings in the isopycnal or height fields (e.g. see the Figure 3 in Toole *et al.* 2011). Although some mixing occurs between the DWBC and the overlying ocean in the northern hemisphere and returns poleward, the core of the DWBC continues to flow southward where it eventually encounters and crosses the equator (e.g. McCartney 1993, McCartney and Curry 1993, Fischer and Schott 1997, Joyce *et al.* 2005, Baehr *et al.* 2009, Cunningham *et al.* 2007).

Oceanographic observations (e.g. Fischer and Schott 1997, Thierry *et al.* 1998, Richardson and Fratantoni 1999, Gouriou *et al.* 2001, Dengler *et al.* 2004) of the DWBC in the equatorial region suggest the following dynamical scenario. As the equator is approached, current speeds in the DWBC increase and are maximum at the equator. The DWBC enters the equatorial region at about 44°W southeast of French Guiana. While some of the water associated with the DWBC continues to flow southward along the coast of Brazil where it breaks up into eddies at about 8°S, the bulk of the DWBC water mass separates from the South American coast at about 35°W, 3°S and turns eastward flowing "swiftly" along the equator. The flow along the equator occurs in a fairly narrow ±3° latitudinal

CONTACT Gordon E. Swaters gswaters@ualberta.ca

band in a topographically constrained equatorial channel located northward of a line of seamounts located along the Fernando de Noronha Ridge. The deepest or abyssal currents in the equatorial channel exhibit meridional oscillations with a wavelength "roughly" on the order of 1000 km. While the mid-Atlantic ridge somewhat disrupts the eastward flow, some of the DWBC water makes its way into the Gulf of Guinea where it is deflected to the south and flows along the African continental slope ultimately making its way into the Indian and eventually Pacific Oceans where it upwells and becomes part of the surface circulation.

Aspects of the qualitative properties listed above are seen in numerical simulations (as described by, e.g. Spall 1994, Borisov and Nof 1998, Nof and Borisov 1998, Edwards and Pedlosky 1998a, 1998b, Kim *et al.* 2014). A key observation made from these simulations is that away from the equator these grounded abyssal flows are, to leading order, inviscid and in planetary-geostrophic balance, that is, to leading order the dominant term in the conserved potential vorticity is f/h, where f is the latitudinally-dependent Coriolis parameter and h is the abyssal layer thickness, respectively. Clearly, since f changes sign at the equator, this suggests that non-conservative or dissipative processes become non-negligible somewhere in the equatorial region in order to permit the cross-equatorial flow of a current that is in planetary geostrophic balance away from the equator on either side of the equator.

Swaters (2013) proposed a nonlinear reduced-gravity model for grounded abyssal flow on a sloping bottom on a rotating sphere (away from the equator) that was in planetary-geostrophic balance and that flowed across the planetary vorticity gradient. The model equations could be solved exactly and an explicit solution obtained. Kim *et al.* (2014) showed that the Swaters (2013) solution was in very good agreement with the midlatitude structure of the numerical solution they obtained from the fully nonlinear shallow water equations for the cross-equatorial flow of a grounded abyssal current on a sloping bottom.

Motivated by the high resolution results of the Kim *et al.* (2014) numerical simulations, Swaters (2015a, 2015b) developed a leading order nonlinear theory for the midlatitude-cross-equatorial flow of grounded abyssal flow on a sloping bottom that shallows on both the western and eastern sides of an ocean basin. The Swaters (2015a, 2015b) model was able to reproduce all of the large-scale inviscid features suggested by the oceanographic observations and numerical simulations (as described above). In particular, Swaters (2015b) showed that when cross-equatorial flow occurs, then necessarily the path-lines or (formally) the characteristics associated with the inviscid solutions intersect in "small isolated" regions near the trough and crest of the nonlinear planetary wave structure (i.e. the equatorial meridional oscillations described above) associated with the eastward flow along the equator of these currents. In the regions where the inviscid characteristics are intersecting the velocity gradients are large and it is in these regions that the requisite dissipation occurs that permits the potential vorticity adjustment required for the cross-equatorial flow of these abyssal flows. The principal purpose of this paper to build on the Swaters (2015a, 2015b) inviscid modelling and give a leading order asymptotic description of the flow characteristics of these cross-equatorial grounded abyssal currents when dissipation can no longer be ignored in the dynamics.

The plan of this paper is as follows. In Section 2 we describe the overall governing equations and provide a very brief overview of the nonlinear inviscid theory as presented by Swaters (2015a, 2015b). In Section 3 we present a multiple-scale model for the onset

of dissipation in the first trough region of the stationary equatorial planetary wave associated with the eastward flow of our DWBC along the equator. We begin by solving the characteristic equations for the flow immediately outside the dissipation zone but inside the "inner inertial equatorial region" as identified by Swaters (2015b). This information is used to determine the appropriate scalings for the solutions in the dissipation regions. We then determine the nonlinear leading order dissipation equations, which we are able to solve exactly. The dissipative solutions regularise the singularities that occur in the velocity gradients and height field in the inviscid solutions as the dissipation region is approached while satisfying all the boundary conditions and smoothly asymptotically matching the inviscid solutions as the dissipation region is exited. The paper is summarised and some concluding remarks are made in Section 4.

2. Model equations and a brief sketch of the inviscid theory

Here, we give an abbreviated description of the nondimensional equations and give a very brief sketch of the principal inviscid results. Full details can be found in Swaters (2015a, 2015b). For the most part, the notation is standard. With horizontal mixing and bottom friction, the nondimensional reduced-gravity equations that describe the midlatitude-equatorial dynamics of a grounded abyssal current on zonally-varying topography can be written in the form

$$\varepsilon\kappa^2\big(u\partial_x + v\partial_y\big)u \,-\, (\sin y)v = -\,(h+h_B)_x + \frac{\varepsilon}{R_E}\big(\partial_{xx} + \kappa^2\partial_{yy}\big)u\,, \tag{1}$$

$$\varepsilon\big(u\partial_x + v\partial_y\big)v \,+\, (\sin y)u = -\,h_y \,+\, \frac{\varepsilon}{\kappa^2 R_E}\big(\partial_{xx} + \kappa^2\partial_{yy}\big)v\,, \tag{2}$$

$$\big(uh\big)_x + \big(vh\big)_y = r\big(\partial_{xx} + \kappa^2\partial_{yy}\big)h\,, \tag{3}$$

where the reduced pressure is $p = h + h_B$, and where

$$h_B\left(x\right) = \frac{1}{2\delta}\left(1-\delta x\right)^2 \qquad \Longrightarrow \qquad h_B'\left(x\right) = -1 + \delta x\,,$$

with

$$\varepsilon \equiv \frac{g's}{4a\Omega^2}\,, \qquad \kappa \equiv \frac{a}{R}\,, \qquad H \equiv \frac{H_*}{sa}\,, \qquad \delta \equiv \frac{a}{x_0} \qquad R_E \equiv \frac{RV}{A_H}\,,$$

where (x, y) are the eastward and northward coordinates, respectively, with corresponding velocities (u, v), respectively, ε is the Rossby number, κ is the aspect ratio between the zonal and meridional length scales (given by a, which is the half width of the abyssal current along the northern boundary in midlatitudes for the northern hemisphere inflow problem (the theory is equally valid for the southern hemisphere inflow problem with the obvious adjustments), and R is the radius of the Earth, respectively; see Figure 1).

Additionally, h_B is the parabolic bottom topography where δ^{-1} is the nondimensional position of the point of maximum depth (dimensionally located at zonal coordinate x_0), s is representative of the bottom slope immediately underneath the abyssal current in midlatitudes, R_E is the Reynolds number, $V = sg'/(2\Omega)$ is the meridional velocity scale, the *Nof speed* (Nof 1983), which is the speed of a steady gravity-driven geostrophically-balanced grounded abyssal water mass on a sloping bottom ($g' = g(\rho_2 - \rho_1)/\rho_2 > 0$ is

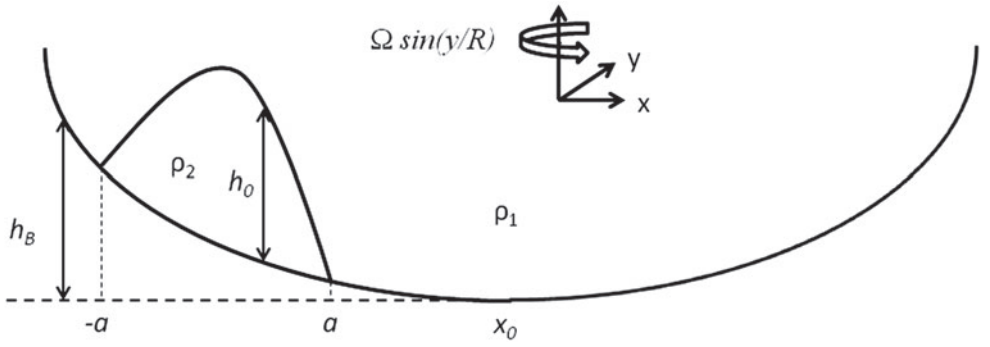

Figure 1. Geometry of the model used in this paper.

the stably-stratified reduced gravity and Ω is Earth's angular frequency 2π rads/day). The parameter r is a nondimensional bottom friction coefficient (we comment more completely on this parameterisation momentarily), and where the DWBC height along the northern boundary $y = y_0$ is given by

$$h(x, y_0) \;=\; h_0\left(x\right) \;\equiv\; \begin{cases} H(1-x^2) & \text{when} \quad |x| \le 1\,, \\ 0 & \text{when} \quad |x| > 1\,, \end{cases} \tag{4}$$

where H is the nondimensional maximum height of the boundary condition (scaled by sa). The usual equatorial β-plane approximation is not introduced into the Coriolis terms in (1) and (2) because we want the solution to be valid well into midlatitudes (where $y \simeq \mathrm{O}(1)$) with a bounded Coriolis parameter (see, e.g. Choboter and Swaters 2004).

Typical values for the parameters appropriate for the DWBC are

$$g' \;\simeq\; 10^{-3}\ \mathrm{m/s^2}\,, \qquad s \;\simeq\; 5.6\times 10^{-3}\,, \qquad a \;\simeq\; 100\ \mathrm{km}\,, \qquad A_H \;\simeq\; 10^2\ \mathrm{m^2/s}\,,$$

which implies that the meridional and zonal velocity scalings are, respectively,

$$V \simeq 3.9\mathrm{cm/s} \qquad \text{and} \qquad Va/R \simeq 0.06\ \mathrm{cm/s}\,,$$

suggesting that

$$\varepsilon \simeq 2.6\times 10^{-3}\,, \qquad \kappa \simeq 1.6\times 10^{-2}\,, \qquad R_E \simeq 2464\,,$$

which suggests that

$$\mathrm{O}\left(\varepsilon^2\right) \lesssim \kappa^2 \simeq R_E^{-1} \lesssim \mathrm{O}(\varepsilon)\,.$$

In addition, the DWBC height scale would be approximately

$$sa \simeq 560\ \mathrm{m} \qquad \Longrightarrow \qquad H \simeq \mathrm{O}(1)\,,$$

and assuming that (at least) $x_0 \simeq 1000$ km, it follows that

$$\mathrm{O}(\varepsilon) \;<\; \delta \;=\; 10^{-1} \;<\; 1\,.$$

The inviscid theory assumes that the Rossby number ε is the underlying asymptotic parameter. Equations (1)–(4) may be thought of as the midlatitude or "outer" asymptotic inertial problem in the limit $0 < \varepsilon \ll 1$.

The rational incorporation of a bottom boundary layer into the mass Equation (3) requires the parameterisation of the vertical velocity at the top of the thin bottom boundary layer in terms of the leading order dynamic pressure in the interior of the DWBC. In midlatitudes (Pedlosky 1987) the vertical velocity at the top of an Ekman bottom boundary layer is proportional to the relative geostrophic vorticity in the interior. On an equatorial β-plane the corresponding theory is more complicated (e.g. Philander 1971) but ultimately results in the vertical velocity at the top of the bottom boundary layer being proportional to the horizontal gradients and second-order derivatives of the interior dynamic pressure. We assume that we can apply the midlatitude parameterisation throughout the domain and simply model the vertical velocity at the top of the bottom boundary layer as proportional to the Laplacian of the interior dynamic pressure associated with the DWBC height. Classical Ekman boundary layer theory coupled to inviscid geostrophic interior dynamics implies that $r \simeq \mathrm{O}(\varepsilon)$ and this will be assumed here too.

We hasten to add that bottom friction is not the only physical process that might degrade the abyssal current height. For example, one such physical process is vertical mixing in which DWBC water becomes entrained into the overlying ocean due to internal gravity wave processes. One is still challenged, however, with how to parameterise these processes in the mass conservation equation. Indeed, it is not unreasonable to model this entrainment degradation with an eddy closure scheme that models the erosion with a scale selective dissipation term proportional to the Laplacian of the height, although other choices are possible. Further observations are required to positively identify the specific mixing processes that we know must occur in the cross-equatorial flow of grounded abyssal water masses.

2.1. Synopsis of the inviscid theory

Swaters (2015a, 2015b) describes the leading order solution to (1)–(3) subject to the boundary condition (4) in the inviscid limit $r = R_E^{-1} = 0$ under a small Rossby number approximation $0 < \varepsilon \ll 1$. As shown by Swaters (2015a), away from the equator the model DWBC corresponds to an equatorward flow along the western boundary predominantly along isobaths across the planetary vorticity gradient (which induces a slight cross-slope component in the velocity field) in which the DWBC height or thickness diminishes and the current speeds up (while conserving meridional volume transport) as the equator is approached (as seen in both shallow water and primitive equation numerical simulations; see, e.g. Spall (1994) and Kim *et al.* (2014)). The midlatitude solution, which corresponds to a non-parallel shear flow, is one of the very few exact results known for meridional flow across the planetary vorticity gradient (see Figure 4 in Swaters 2013, Figure 7(a) in Kim *et al.* (2014) and Figure 3 in Swaters 2015a). As described in Swaters (2013, 2015a), provided $v(x, y_0)$ is equatorward (regardless of the source hemisphere) no shock will form in the solution in midlatitudes and we are assured that the midlatitude solution will be smooth until it reaches the equatorial region. However, the midlatitude inviscid velocities become singular as the equator is approached with the asymptotic behaviour as a consequence of the planetary geostrophic balance.

As the midlatitude flow approaches the equator the singular behaviour in the inviscid velocities suggests that nonlinearity becomes increasingly important in the momentum equations. Swaters (2015a) has shown that the first distinguished limit occurs when the meridional flux of meridional momentum term is as important as the geostrophic balance and this occurs when $y \approx \mathrm{O}\left(\varepsilon^{1/3}\right)$ (or, dimensionally, in a zonal band with half width of order 900 km centred along the equator). The solution in this so-called "intermediate" equatorial region describes the transition or turning of the DWBC from a north–south meridional flow into a eastward zonal equatorial jet (see Figure 7 in Swaters 2015a).

However, while having described the important physical requirement of turning the equatorward midlatitude flow into a zonal equatorially-constrained eastward jet (valid whether the inflow hemisphere is the northern or southern hemisphere, and while conserving meridional volume transport), the "intermediate" equatorial region solution describes a flow that continues to "speed up" (consistent with the observations) as the equator is approached and thus the singularities in the inviscid velocities as the equator is approached remain. This unphysical behaviour suggests the emergence of yet another nonlinear inviscid inertial boundary layer as the flow approaches equator in which the unbounded singularities in the velocity are resolved. Swaters (2015b) has shown that a second distinguished inertial limit occurs when all the nonlinear terms in the momentum equations are as important as the geostrophic balance and this occurs when $y \approx \mathrm{O}\left((\varepsilon\kappa)^{1/3}\right)$ (or, dimensionally, in a zonal band with half width of order 200 km centred along the equator). It is in this so-called "inner" equatorial region that the inviscid velocities are regularised in the sense that they no longer become unbounded.

As shown by Swaters (2015b), the inviscid cross-equatorial current in the inner equatorial region corresponds to a predominately zonal jet that meanders meridionally as the DWBC flows eastward (see Figure 1 in Swaters 2015b). The "wavelength" of these meanders is about 1800 km, which is consistent with the oceanographic observations as described above. These meanders are an intrinsically nonlinear stationary planetary wave that develops as the DWBC first "overshoots" the equator in the western side of the basin with PV conservation on an equatorial β-plane subsequently attempting to rectify the flow. In the context of the large scale inviscid structure, because energy is conserved and potential energy is acquired as the flow moves up the slope on the eastern side of the basin, the current reaches a maximum eastward extent upon which it must exit the equatorial region and re-orient itself as poleward flowing grounded abyssal current along the eastern boundary (see, as well, Figures 4 and 6 in Kim *et al.* 2014) first transiting back through an "intermediate" equatorial region and then, to leading order, described by the above midlatitude dynamics.

Further, Swaters (2015b) showed that in "isolated" regions or patches near the crest and trough of the stationary planetary wave the characteristics associated with the inviscid solutions necessarily intersect (at least once) if genuine cross-equatorial flow occurs. In the regions where the characteristics are intersecting the spatial gradients of the otherwise bounded velocities become very large and it is in these regions that dissipation cannot be neglected. Our goal here is to determine the spatial structure of the steady velocity and height fields when dissipation is introduced into the "inner" equatorial region equations.

2.2. "Inner" equatorial region equations with dissipation

The scalings for the "inner" equatorial region (careted) variables are given by (Swaters 2015b)

$$u = (\varepsilon\kappa^4)^{-1/3}\widehat{u}(x,\zeta), \qquad v = (\varepsilon\kappa)^{-1/3}\widehat{v}(x,\zeta),$$
$$h = (\varepsilon\kappa)^{1/3}\widehat{h}(x,\zeta), \qquad \text{and} \qquad y = (\varepsilon\kappa)^{1/3}\zeta, \tag{5}$$

which when substituted into (1)–(3), yields

$$\nu\widehat{u}\widehat{u}_x + \widehat{v}\widehat{u}_\zeta - \frac{\sin\left((\kappa\varepsilon)^{1/3}\zeta\right)}{(\kappa\varepsilon)^{1/3}}\widehat{v} = -\left(h_B + (\kappa\varepsilon)^{1/3}\widehat{h}\right)_x + \frac{1}{R_E}\left(\nu^2\partial_{xx} + \partial_{\zeta\zeta}\right)\widehat{u}, \tag{6}$$

$$\nu\widehat{u}\widehat{v}_x + \widehat{v}\widehat{v}_\zeta + \frac{\sin\left((\kappa\varepsilon)^{1/3}\zeta\right)}{(\kappa\varepsilon)^{1/3}}\widehat{u} = -\kappa\widehat{h}_\zeta + \frac{1}{R_E}\left(\nu^2\partial_{xx} + \partial_{\zeta\zeta}\right)\widehat{v}, \tag{7}$$

$$\nu\left(\widehat{u}\widehat{h}\right)_x + \left(\widehat{v}\widehat{h}\right)_\zeta = \widehat{r}\left(\nu^2\partial_{xx} + \partial_{\zeta\zeta}\right)\widehat{h}, \tag{8}$$

where

$$\nu \equiv \left(\varepsilon/\kappa^2\right)^{1/3} \simeq 2.21 \simeq \mathrm{O}(1) \qquad \text{and} \qquad \widehat{r} \equiv r\kappa^2. \tag{9}$$

To leading order in the Rossby number ε, (5)–(7) reduce to the quasi-linear equatorial β-plane equations, given by

$$\left(\nu u\partial_x + v\partial_\zeta\right)u - \zeta v = -h_B'(x) + \frac{1}{R_E}\left(\nu^2\partial_{xx} + \partial_{\zeta\zeta}\right)u, \tag{10}$$

$$\left(\nu u\partial_x + v\partial_\zeta\right)v + \zeta u = -\kappa h_\zeta + \frac{1}{R_E}\left(\nu^2\partial_{xx} + \partial_{\zeta\zeta}\right)v, \tag{11}$$

$$\nu(uh)_x + (vh)_\zeta = \widehat{r}\left(\nu^2\partial_{xx} + \partial_{\zeta\zeta}\right)h, \tag{12}$$

and where for convenience we have dropped the carets on u, v and h. These equations must be must be solved subject to the asymptotic matching conditions

$$u \to \frac{\left(h_B'(x)\right)^2}{\zeta^4}, \qquad v \to \frac{h_B'(x)}{\zeta}, \qquad h \to \frac{\zeta\, h_0\left(\tau(x)\right)}{\sin y_0}, \tag{13}$$

where

$$\tau(x) = \begin{cases} \dfrac{1 - \sqrt{1 + 2\left(2H - \delta\right)\left(H + x - \delta x^2/2\right)}}{\delta - 2H} & \text{for} \quad |x| \le 1, \\ x & \text{for} \quad |x| > 1, \end{cases}$$

as $\zeta \to \infty$ (in the northern hemisphere, $\zeta \to -\infty$ in the southern hemisphere). The matching conditions (13) follows from the leading order behaviour of the "intermediate" equatorial region solutions as they enter the "inner" equatorial region (see Equations (11)–(13) in Swaters 2015b).

The Swaters (2015b) inviscid model corresponds to (10)–(12) with $\widehat{r} = R_E^{-1} = 0$. In addition, the Swaters (2015b) inviscid model also neglects the pressure gradient term

κh_ζ in (11). This is asymptotically rigorous in the small Rossby number approximation since our scalings suggest that $O(\varepsilon) \lesssim \kappa \lesssim O(\varepsilon^{1/2})$ provided that h_ζ remains bounded, which Swaters (2015b) has shown to be the case for the inviscid solutions outside of the dissipation regions. However, as the inviscid solutions enter the dissipation regions h_ζ becomes unbounded and care must be taken with this term (as described below).

In full generality, solving (10)–(12) subject to (13) appears to be analytically intractable. We have been able to make substantial analytic progress, however, in the context of a simpler set of equations in which we exploit the "slowly varying" slope of the bottom topography as the DWBC approaches the first dissipation region. It is to this approximate dissipative model and its solution that we now turn our attention to.

3. An approximate model for the flow into and within the first dissipation region

In this section we introduce a multiple-scale boundary layer model in order to determine the leading order spatial structure of the velocity and height fields in the first dissipation region, or region with intersecting characteristics, associated with the first trough in the stationary planetary wave that develops in the inner equatorial region. This analysis is built on classical matched asymptotic expansions and nonlinear internal viscous boundary layer theory (see, e.g. Bender and Orszag 1978).

Examining (10), (11) and (13) we see that the x-variations in v and u are a consequence of $h_B'(x) = -1 + \delta x$ where $\delta \simeq O(10^{-1})$ whereas the leading order x-variations in h will be set by (12) and (13), which will vary on a, comparatively, faster $O(1)$ x-scale. In addition, Swaters (2015b) has shown that the first dissipation zone, positioned near the first trough in the planetary wave is located approximately near $x \simeq 5$ (see Figures 2 and 6 in Swaters 2015b). This suggests introducing a multiple-scale *ansatz* in which the long spatial variable $X = \delta x$ is defined so that we can separate out the x-variations in the solution induced by the curvature in the topography from those induced by the cross-slope shape of the inflowing DWBC.

Our approach to the problem will be to first determine the leading order inviscid solution in the inner equatorial region but outside the dissipation zone in this approximate model. Based on this solution we will be able to explicitly determine the leading order spatial structure of the DWBC as it enters the region where the characteristics are intersecting. Based on this additional information we can then determine the appropriate scalings and leading order dissipation equations and explicitly solve those equations with solutions that asymptotically match the solutions in the inner equatorial region but outside the dissipation zone.

The introduction of the stretched or boundary layer variable $X = \delta x$ means that x-derivatives will map according to

$$\partial_x \to \partial_x + \delta \partial_X,$$

and assuming a multiple-scale solution in the inner equatorial region of the form

$$u = u(x, \zeta; X), \qquad v = v(x, \zeta; X) \qquad \text{and} \qquad h = h(x, \zeta; X),$$

leads to, after substituting into (10)–(12), the equations

$$\begin{aligned}
\big(v u\partial_x + \delta v u\partial_X + v\partial_\zeta\big)u - \zeta v &= -\gamma(X) + \frac{1}{R_E}\big(v^2\partial_{xx} + 2\delta v^2\partial_{Xx} + \partial_{\zeta\zeta}\big)u + \mathrm{O}\big(\delta^2\big),\\
\big(v u\partial_x + \delta v u\partial_X + v_\zeta\big)v + \zeta u &= -\kappa h_\zeta + \frac{1}{R_E}\big(v^2\partial_{xx} + 2\delta v^2\partial_{Xx} + \partial_{\zeta\zeta}\big)v + \mathrm{O}\big(\delta^2\big),\\
v(uh)_x + \delta v(uh)_X + (vh)_\zeta &= \widehat{r}\big(v^2\partial_{xx} + 2\delta v^2\partial_{Xx} + \partial_{\zeta\zeta}\big)h + \mathrm{O}\big(\delta^2\big),
\end{aligned}$$

where $h_B' = \gamma\left(X\right) \equiv -1 + X$.

To leading order in δ, these equations reduce to simply

$$\big(v u\partial_x + v\partial_\zeta\big)u - \zeta v = -\gamma(X) + \frac{1}{R_E}\big(v^2\partial_{xx} + \partial_{\zeta\zeta}\big)u\,, \tag{14}$$

$$\big(v u\partial_x + v\partial_\zeta\big)v + \zeta u = -\kappa h_\zeta + \frac{1}{R_E}\big(v^2\partial_{xx} + \partial_{\zeta\zeta}\big)v\,, \tag{15}$$

$$v(uh)_x + (vh)_\zeta = \widehat{r}\,\big(v^2\partial_{xx} + \partial_{\zeta\zeta}\big)h\,, \tag{16}$$

which must be solved subject to the formal asymptotic matching conditions (see (13))

$$h \to \frac{\zeta\, h_0\big(\widehat{\tau}(x)\big)}{\sin y_0}\,, \qquad u \to \frac{\big(\gamma(X)\big)^2}{\zeta^4}\,, \qquad v \to \frac{\gamma(X)}{\zeta}\,, \tag{17}$$

as $\zeta \to \infty$ (for a flow originating in the northern hemisphere), where $\widehat{\tau}\left(x\right)$ is the $\delta \to 0$ limit of $\tau\left(x\right)$, which is explicitly given by

$$\widehat{\tau}(x) = \begin{cases} \dfrac{\sqrt{4H^2 + 4Hx + 1} - 1}{2H} & \text{for} \quad |x| \le 1,\\[2ex] x & \text{for} \quad |x| > 1, \end{cases} \tag{18}$$

where it is assumed that $H < 1/2$ (this is the $\delta \to 0$ limit of the no midlatitude shock condition, see Swaters 2015a).

From the perspective of the multiple-scale ansatz, the effect of the varying slope in the bottom topography will now be parameterically represented in the leading order equations. The fact that the pressure gradient term in (14) and the matching conditions for $\left(u, v\right)$ in (17) depend only on X will mean that the solutions for $\left(u, v\right)$ will be, as we show below, independent of x. This significantly simplifies the solution.

3.1. The leading order solution outside the first dissipation region

Outside the dissipation region the flow is to leading order inviscid and (14) and (15) reduce to

$$\begin{aligned}
\big(v u\partial_x + v\partial_\zeta\big)u - \zeta v &= -\gamma(X)\,,\\
\big(v u\partial_x + v\partial_\zeta\big)v + \zeta u &= 0,
\end{aligned}$$

where, on account of $\mathrm{O}(\varepsilon) \lesssim \kappa \lesssim \mathrm{O}(\varepsilon^{1/2})$, the h_ζ term in (15) is neglected in the inviscid region. These can be solved using the method of characteristics. The characteristic equations associated with this multiple-scale model are given by

$$\frac{\mathrm{d}x}{\mathrm{d}\sigma} = \nu u\,, \qquad \frac{\mathrm{d}\zeta}{\mathrm{d}\sigma} = \nu\,, \tag{19}$$

$$\frac{\mathrm{d}u}{\mathrm{d}\sigma} - \zeta\nu = -\gamma(X)\,, \qquad \frac{\mathrm{d}\nu}{\mathrm{d}\sigma} + \zeta u = 0\,, \tag{20}$$

which will be solved subject to the (northern) boundary conditions

$$x|_{\sigma=0} = \mu\,, \qquad \zeta|_{\sigma=0} = \zeta_0 = \frac{1+\kappa^{1/3}}{2\kappa^{1/3}} = 2.5\,, \tag{21}$$

$$u|_{\sigma=0} = \frac{\gamma^2(X)}{\zeta_0^4}\,, \qquad \nu|_{\sigma=0} = \frac{\gamma(X)}{\zeta_0}\,, \tag{22}$$

where σ is the coordinate along the characteristics and $-1 \le \mu \le 1$ is the coordinate across the characteristics. The coordinate μ parameterises the dependence (if any) of the boundary data along the boundary curve $\zeta = \zeta_0$ with respect to x. The characteristics will be the curves in (x, ζ)-space for which μ is constant. In order to numerically compute the characteristics it is necessary to "start" the solution at a finite value of ζ. The choice of ζ_0 in (21) corresponds, formally, to a value that is "outside" the inner equatorial region but "inside" the intermediate equatorial region (Swaters 2015b). The qualitative behaviour of the numerical solution is not sensitive to the particular choice of ζ_0 (Swaters 2015b).

Substitution of (19b) into (20a) followed by an integration with respect to σ (for a similar derivation in the context of a Lagrangian-particle model see Cushman-Roisin 1982) yields the angular momentum balance

$$u = \frac{\zeta^2}{2} - \gamma(X)\sigma + \frac{\gamma^2(X)}{\zeta_0^4} - \frac{\zeta_0^2}{2}\,, \tag{23}$$

which together with (19b) and (20b) implies that ζ will be determined from

$$\frac{\mathrm{d}^2\zeta}{\mathrm{d}\sigma^2} + \left[\frac{\zeta^2}{2} - \gamma(X)\,\sigma + \frac{\gamma^2(X)}{\zeta_0^4} - \frac{\zeta_0^2}{2}\right]\zeta = 0\,,$$

$$\zeta|_{\sigma=0} = \zeta_0\,, \qquad \left.\frac{\mathrm{d}\zeta}{\mathrm{d}\sigma}\right|_{\sigma=0} = \frac{\gamma(X)}{\zeta_0}\,. \tag{24}$$

Equations (19), (23) and (24) imply that u, ν and ζ depend *only* on σ and X (and not on μ) so that we may write $u = u(\sigma; X)$, $\nu = \nu(\sigma; X)$ and $\zeta = \zeta(\sigma; X)$. Consequently, it follows from (19a) and (21a) that

$$x = \mu + \nu \int_0^\sigma u(\eta; X)\,\mathrm{d}\eta\,, \tag{25}$$

Finally, to determine the explicit dependence of u and ν on ζ and X (there is no dependence on x), one would formally invert $\zeta = \zeta(\sigma; X)$ to obtain $\sigma = \sigma(\zeta; X)$ and substitute into $u(\sigma; X)$ and $\nu(\sigma; X)$.

The only known analytical solution to (24) is for $\gamma = 0$ (a flat bottom). However, in the case where $\gamma = 0$, the solution to this multiple-scale model is trivial (underscoring the importance of the downslope gravitational acceleration in driving the flow in the inner equatorial region; the same conclusion is true for the full model, see Swaters 2015b). This follows from energy conservation and the initial conditions. The energy equation associated with (19) and (20) can be written in the form

$$\left(\frac{u^2+v^2}{2} + \frac{1}{\delta v}\int_1^{\delta x} \gamma(z)\,\mathrm{d}z\right)_\sigma = 0\,. \tag{26}$$

Thus when $\gamma = 0$, (26) and (22) implies that $u = v = 0$. It further follows from (24) and (25) that $(x,\zeta) = (\mu,\zeta_0)$. When $\gamma \neq 0$, there is no known analytical solution to (24) and it must be solved numerically.

With the velocities determined we can explicitly solve for h. Given that u and v depend only on ζ and X implies that the mass conservation Equation (16) (in the inviscid limit) reduces to

$$vuh_x + (vh)_\zeta = 0\,,$$

or, equivalently after multiplication by v,

$$\left(vu\partial_x + v\partial_\zeta\right)(vh) = 0\,, \tag{27}$$

which can be shown to be just the PV equation for this approximate model. In terms of the characteristic coordinates (μ,σ), (27) reduces to simply

$$(vh)_\sigma = 0\,,$$

(implying that the meridional volume flux is conserved along the characteristics in the inner equatorial region), which must be solved subject to (see (17))

$$h\big|_{\sigma=0} = \frac{\zeta_0\, h_0\big(\widehat{\tau}(\mu)\big)}{\sin y_0}\,, \tag{28}$$

the solution of which can be written in the form

$$h(\mu,\sigma;X) = \frac{\gamma(X) h_0\big(\widehat{\tau}(\mu)\big)}{v(\sigma;X)\sin y_0}\,, \tag{29}$$

where (22b) has been used.

Hence we have, formally at least, completely determined the spatial structure of the DWBC for this approximate model in the inviscid inner equatorial region just prior to the onset of intersecting characteristics, which corresponds to the point at which dissipation cannot be neglected. We now turn to determining the conditions for the onset of intersecting characteristics associated with these solutions.

The characteristics begin to intersect, that is the inviscid spatial gradients $|u_\zeta| \sim |v_\zeta| \to \infty$ or, physically, dissipation becomes important, when the Jacobian associated with the transformation from the Cartesian coordinates (x,ζ) to the characteristic coordinates

(σ, μ) is zero, i.e.

$$\partial(\mu,\sigma) \equiv \begin{vmatrix} x_\sigma & x_\mu \\ \zeta_\sigma & \zeta_\mu \end{vmatrix} = \begin{vmatrix} \nu u & 1 \\ \nu & 0 \end{vmatrix} = -\nu(\sigma; X) = 0\,. \tag{30}$$

Thus, within the context of the approximate model examined here, when $\nu = 0$ we expect dissipation to become important in the physics. Since $\nu = 0$ at the first trough of the stationary planetary wave, this approximate model will locate the first dissipation zone near the first trough of the stationary wave, which is similar to the results obtained from the full model (Swaters 2015b). Moreover, the point at which $\nu = 0$ corresponds to the southern most extent of each characteristic or pathline since the flow begins to turn around and flow back north toward the equator once $\nu = 0$ occurs (see Figure 1 in Swaters 2015b). This means that the locus of the points associated with the singularity in the spatial gradients in the velocity along each path line *is* located along the southern edge of the DWBC, i.e. the singularity in the inviscid solution forms on the southern grounding of the DWBC as it enters the southern hemisphere and begins to flow back northward. These facts set the appropriate boundary conditions to use for the dissipative solutions.

Formally, $\nu(\sigma; X) = 0$ defines the relationship

$$\sigma \equiv \sigma_\triangle(X)\,,$$

which specifies the value of σ as a function of X associated with the onset of the singularity in the velocity gradients in the inviscid solution. The x and ζ coordinates associated with where $\nu(\sigma; X) = 0$ will therefore be given by, respectively,

$$\begin{aligned} x &= x_s(\mu, X) \equiv x\big(\mu, \sigma_\triangle(X); X\big)\,, \\ \zeta &= \zeta_s(X) \equiv \zeta\big(\sigma_\triangle(X); X\big), \end{aligned}$$

where $\zeta(\sigma; X)$ and $x(\mu, \sigma; X)$ are determined by (24) and (25), respectively. Although the x and ζ coordinates associated with where $\nu(\sigma; X) = 0$ have a slow dependency on variations in the bottom slope, and the x coordinate associated with where $\nu(\sigma; X) = 0$ depends explicitly on the specific characteristic μ, the onset of intersecting characteristics is in the immediate neighbourhood of $x = x_s(0, 0) \simeq 5.75$ and $\zeta = \zeta_s(0) \simeq -0.79$ (see Figure 2). The values of (x_s, ζ_s) for other values of μ are very similar. Calculations show that (x_s, ζ_s) lie in the relatively small band or region $5.0 \lesssim x_s \lesssim 6.5$ and $-0.81 \lesssim \zeta_s \lesssim -0.76$. Given that the zonal length scale is 100 km and the dimensional scaling for ζ is 220 km, this suggests that the region of intersecting characteristics, or where the dissipation is important, occurs in zonal band that is about 11 km wide meridionally with a zonal length of about 150 km, which is located at the first trough in the stationary planetary wave, which is itself located about 175 km south of the equator (see Figure 2).

Figure 2 is a contour plot of the characteristic curves $\big(x(\mu, \sigma; \delta\mu), \zeta(\sigma; \delta\mu)\big)$, as determined by (24) and (25), (numerically computed using *Mathematica*) for (moving from left to right along $\zeta = 2.5$) $\mu = -1.0$ (solid contour; the initially most westerly characteristic, see (18) and (28)), -0.5 (dotted contour), 0.0 (dashed contour), 0.5 (dot-dashed contour) and 1.0 (large-dashed contour; the initially most easterly characteristic), respectively, for $-2 < x < 9$ (the right-hand end point of this interval is slightly to the east of the point of singularity formation on the initially most easterly $\mu = 1$ characteristic). Figure 2 is

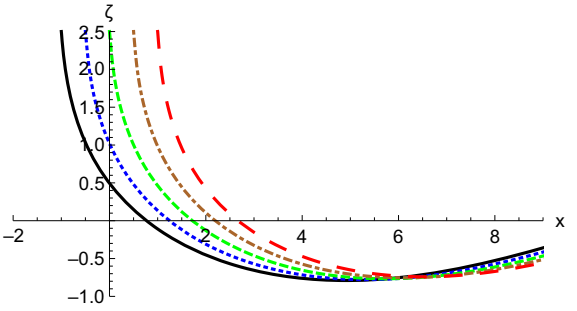

Figure 2. The characteristic curves $\big(x(\mu,\sigma;\delta\mu),\zeta(\sigma;\delta\mu)\big)$for $\mu = -1.0, -0.5, 0.0, 0.5$ and 1.0.

qualitatively similar to Figure 1 in Swaters (2015b) (which was computed for the full model without the multiple-scale ansatz made here) over the region of interest. At the trough point on each characteristic it follows $v = 0$ and it is at this point that dissipation can no longer be neglected. We have seen that $x_s(0,0) \simeq 5.75$ and from Figure 2 we see that $\mu = 0$ (the green contour) crosses the equator ($\zeta = 0$) at about $x \simeq 1.75$. Since the zonal length scale is 100 km, this suggests that region of intersecting characteristics is approximately located about 400 km to the east of where the DWBC first crosses the equator.

Figure 3(a) and (b) shows graphs, respectively, of u and v vs. ζ on the $\mu = 0$ characteristic (we also set $X = 0$) for the range $-0.77 \simeq \zeta_s(0) \leq \zeta \leq \zeta_0$, i.e. over the range of ζ values for which $v \leq 0$. Figure 3(a) shows u monotonically increasing, but remaining bounded, as ζ decreases toward $\zeta_s(0)$. At the point of singularity $\zeta = \zeta_s(0)$, where $|u_\zeta| \to \infty$, it follows that $u = u_s \simeq 2.31$. Figure 3(b) shows v initially decreasing, but remaining bounded, as ζ decreases and then rapidly increasing until the point of singularity $\zeta = \zeta_s(0)$, where $v = 0$ but $|v_\zeta| \to \infty$, is reached. We note that since $\zeta = 1$ corresponds, dimensionally, to about 221 km, it follows that $\zeta_s(0) \simeq -0.77$ corresponds to a point that is about 170.2 km south of the equator. The qualitative structure of $u(\sigma;X)$ and $v(\sigma;X)$ varies slowly across the characteristics, i.e. graphs for $u(\sigma;X)$ and $v(\sigma;X)$ are very similar to Figure 3(a) and (b) for $-0.1 \leq X \leq 0.1$.

Figure 3(c) shows a graph of h vs. x, as determined by (29), along the $\mu = 0$ characteristic for the range $0 \leq x < x_s(0;0) \simeq 5.75$ (and is very similar to Figure 7 in Swaters (2015b), which was obtained without the multiple-scale approximation used here). The graphs for h along other characteristics are qualitatively similar. In accordance with (29), the onset of intersecting characteristics, i.e. $v = 0$, means that the inviscid solution for h becomes unbounded. This unphysical behaviour is rectified when dissipation is introduced.

Finally, it is possible to determine the leading order asymptotic structure of $u(\zeta;X)$ and $v(\zeta;X)$ near the point of singularity $\zeta = \zeta_s(X)$ and to use this information to determine the appropriate scaling for the leading order dissipation problem. It follows from (14) and (15) (in the inviscid limit) that, to leading order, for ζ "near" $\zeta_s(X)$

$$vu_\zeta = -\gamma\,, \tag{31}$$

$$vv_\zeta = -\zeta_s u_s\,, \tag{32}$$

(since $v(\zeta_s;X) = 0$ and u and v do not depend on x) where $u_s = u(\zeta_s;X)$.

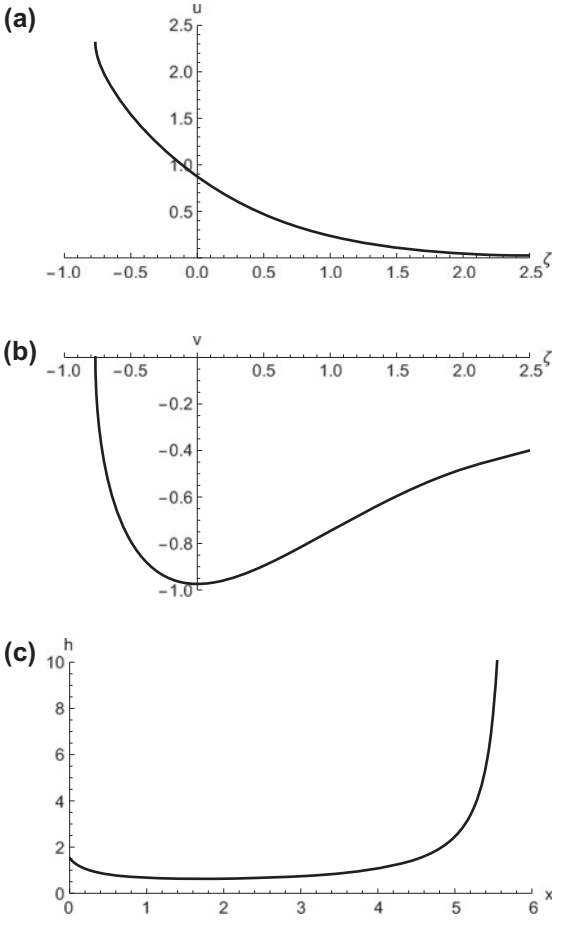

Figure 3. Graphs of (a) u vs. ζ, (b) v vs. ζ, and (c) h vs. x; each along the $\mu = 0$ characteristic.

Equation (32) can be integrated to imply that, to leading order, as $\zeta \to \zeta_s^+ < 0$

$$v = -\sqrt{-2\zeta_s u_s(\zeta - \zeta_s)}\,, \tag{33}$$

which, in turn, implies from (31) that

$$u = u_s + \gamma\sqrt{-2(\zeta - \zeta_s)/(\zeta_s u_s)}\,, \tag{34}$$

where we have imposed the boundary conditions that $v = 0$ and $u = u_s$ when $\zeta = \zeta_s$ (and selected the minus root associated with v so that $v < 0$ for $\zeta \to \zeta_s^+$). Consequently, we conclude that as $\zeta \to \zeta_s^+$,

$$|v| \sim |u - u_s| \simeq \mathrm{O}\big((\zeta - \zeta_s)^{1/2}\big)\,, \tag{35}$$

$$\big|u_\zeta\big| \sim \big|v_\zeta\big| \simeq \mathrm{O}\big((\zeta - \zeta_s)^{-1/2}\big)\,, \qquad \big|u_{\zeta\zeta}\big| \sim \big|v_{\zeta\zeta}\big| \simeq \mathrm{O}\big((\zeta - \zeta_s)^{-3/2}\big)\,. \tag{36}$$

Similarly, it follows from (29) that

$$|h| \simeq \mathrm{O}\big((\zeta - \zeta_s)^{-1/2}\big), \qquad \big|h_{\zeta\zeta}\big| \simeq \mathrm{O}\big((\zeta - \zeta_s)^{-5/2}\big) \qquad \text{as} \quad \zeta \to \zeta_s^+. \tag{37}$$

From (33) and (34) we see that the inviscid velocities remain continuous and bounded on each individual characteristic as the region with intersecting characteristics is entered. Formally, however, the solutions for u and v become multi-valued across the characteristics (Swaters 2015b) as $\zeta \to \zeta_s^+$. As shown by (36) and (37) the velocity gradients u_ζ and v_ζ and the height h (and their higher order derivatives) become singular as $\zeta \to \zeta_s^+$. This unphysical behaviour is rectified by horizontal mixing and bottom friction (there may be other physical processes that could accomplish the same objective). It is to that end that we now turn our attention to The asymptotic structure (33)–(37) is critical in determining the scalings associated with the leading order dissipation problem for $\zeta \simeq \zeta_s^+$.

3.2. The leading order velocity within the first dissipation region

Under the multiple-scale ansatz adopted for our approximate dissipation model in which to leading order u and v do not depend on x, it follows from (14) and (15) that the leading order nonlinear momentum equations for the inner equatorial region with dissipation included will be given by

$$vu_\zeta - \zeta v = -\gamma + \frac{1}{R_E} u_{\zeta\zeta}\,, \tag{38}$$

$$vv_\zeta + \zeta u = -\kappa h_\zeta + \frac{1}{R_E} v_{\zeta\zeta}\,. \tag{39}$$

Based on the asymptotic behaviour (33)–(36) as $\zeta \to \zeta_s^+$, it follows that the dissipative terms in (38) and (39) will make an O(1) contribution to the dynamics when $|\zeta - \zeta_s| \simeq \mathrm{O}\big(R_E^{-2/3}\big)$. Given that O(1) variations in ζ correspond, dimensionally, to about 220 km and that our choice for the horizontal eddy viscosity (see Swaters 2015a) implies a Reynolds number $R_E \simeq 2464$, it follows the dissipation length scale at the point of singularity will be on the order of 1.2 km. The dissipation length scale increases with increasing horizontal eddy viscosity. For example, if we assume $A_H = 10^3$ m^2/s (an increase by a factor of 10), the dissipation length scale increases to about 5.6 km.

Based on this scale analysis and (33)–(37), the dissipation boundary layer variables χ, $\widetilde{u}$, $\widetilde{v}$ and $\widetilde{h}$ appropriate near the point of singularity, will be given by

$$\zeta = \zeta_s + \chi/R_E^{2/3}, \qquad u = u_s + \widetilde{u}/R_E^{1/3}, \qquad v = \widetilde{v}/R_E^{1/3}, \qquad h = R_E^{1/3}\widetilde{h}\,, \tag{40}$$

(so that $\zeta \geq \zeta_s^+ \Longleftrightarrow \chi \geq 0$ and that $u \to u_s$ as $\zeta \to \zeta_s^+ \Longleftrightarrow \widetilde{u} \to 0$ as $\chi \to 0^+$) which when substituted into the momentum Equations (38) and (39) yields (after dropping the tildes)

$$vu_\chi - \big(\zeta_s + \chi/R_E^{2/3}\big)v/R_E^{1/3} = -\gamma + u_{\chi\chi}, \tag{41}$$

$$vv_\chi + \big(\zeta_s + \chi/R_E^{2/3}\big)\big(u_s + u/R_E^{1/3}\big) = -\kappa R_E h_\chi + v_{\chi\chi}, \tag{42}$$

Formally, the coefficient $\kappa R_E \simeq \mathrm{O}(1)$ in (42) and so cannot be assumed to be small. However, much can be learned if we neglect this term. In particular, we are able to completely solve the leading order dissipation equations and obtain bounded solutions that smoothly satisfy all the boundary conditions and exactly asymptotically match with the inviscid solutions obtained previously in this section for the inviscid inner equatorial region outside the dissipation zone. In fact, the solutions so obtained will possess the property that h_χ is bounded for all χ and that $h_\chi \to 0$ as $\chi \to \infty$ (exiting the dissipation region). Based on this *a posteriori* information, we will neglect this term. Thus, to leading order, (41) and (42) will reduce to

$$\nu u_\chi = -\gamma + u_{\chi\chi}\,, \tag{43}$$

$$\nu v_\chi + \zeta_s u_s = v_{\chi\chi}\,. \tag{44}$$

These are identical in form to (31) and (32) but with dissipation included.

Equation (44) can be immediately integrated to yield

$$v_\chi = \tfrac{1}{2}v^2 + \zeta_s u_s \chi\,, \tag{45}$$

where we have imposed the boundary condition $v_\chi(0) = 0$, i.e. we assume that $v \to 0$ *smoothly* as $\chi \to 0^+$. Equation (45) can be transformed into *Airy's* equation if the change of variables

$$\chi = \sqrt[3]{-2/\left(\zeta_s u_s\right)}\, z\,, \qquad \text{and} \qquad v = \sqrt[3]{-4\zeta_s u_s}\,\varphi(z)\,,$$

is introduced into (45), yielding

$$\varphi_z = \varphi^2 - z\,, \tag{46}$$

and if the *Cole-Hopf* transformation

$$\varphi = -\psi_z/\psi\,,$$

is introduced into (46) yielding *Airy's* equation in the form

$$\psi_{zz} - z\psi = 0\,, \tag{47}$$

where it is recalled that $z \to 0^+ \Longleftrightarrow \zeta \to \zeta_s^+ < 0$.

The general solution to (47) is given by

$$\psi(z) = c_1\,\mathrm{Ai}\,(z) + c_2\,\mathrm{Bi}\,(z)\,,$$

where $\mathrm{Ai}\,(z)$ and $\mathrm{Bi}\,(z)$ are the *Airy* functions of the first and second kind, respectively, and $c_{1,2}$ are arbitrary constants, implying that the general solution for φ is given by

$$\varphi(z) = -\frac{c\,\mathrm{Ai}'\,(z) + \mathrm{Bi}'\,(z)}{c\,\mathrm{Ai}\,(z) + \mathrm{Bi}\,(z)}\,,$$

where c is a free constant and "prime" means differentiation with respect to the argument. The constant c is chosen so that $\varphi(0) = 0 \Longleftrightarrow v(\zeta_s; X) = 0$, implying that (Abramowitz and Stegun 1970)

$$c \;=\; -\,\mathrm{Bi}'\,(0)\big/\,\mathrm{Ai}'\,(0) \;=\; \sqrt{3}\,.$$

Thus, we find that

$$\varphi(z) \;=\; -\,\frac{\sqrt{3}\,\mathrm{Ai}'\,(z)+\mathrm{Bi}'\,(z)}{\sqrt{3}\,\mathrm{Ai}\,(z)+\mathrm{Bi}\,(z)}\,. \tag{48}$$

Hence, the solution to (45) can be written in the form

$$v \;=\; \sqrt[3]{-4\zeta_s u_s}\;\varphi\big(\sqrt[3]{-\zeta_s u_s/2}\;\chi\big). \tag{49}$$

In summary, the leading order solution for (39), valid for $\zeta \simeq \zeta_s^+$ and $0 < R_E^{-1} \ll 1$ (and neglecting the $\mathrm{O}(\kappa)$ pressure gradient term), written in terms of the "outer" inviscid variables (within the inner equatorial region) ζ and v in (39), will be given by

$$v \;=\; \sqrt[3]{-4\zeta_s u_s/R_E}\;\varphi\left(\sqrt[3]{-\zeta_s u_s R_E^2/2}\;(\zeta-\zeta_s)\right). \tag{50}$$

It can be shown that the solution (50) asymptotically exactly matches, as $R_E \to \infty$, the inviscid "outer" solution (33). Thus, we have found a solution for v near the region of the point of inviscid singularity for the gradient u_ζ that is no longer singular when dissipation is included.

Finally, the uniformly valid leading order solution for v, valid *both* in the "outer" inviscid region and in the dissipation region (all within the inner equatorial region), will be given by

$$v_{\mathrm{unif}} \;=\; v\big(\sigma(\zeta)\big) + \sqrt[3]{-4\zeta_s u_s/R_E}\;\varphi\left(\sqrt[3]{-\zeta_s u_s R_E^2/2}\;(\zeta-\zeta_s)\right) + \sqrt{-2\zeta_s u_s(\zeta-\zeta_s)}\,, \tag{51}$$

where $v\big(\sigma(\zeta)\big)$ is determined by (19) and (24) with $\sigma(\zeta)$ the inverse function associated with $\zeta = \zeta(\sigma)$ where ζ is determined by (24), and where we have suppressed, purely for convenience, the notational dependence on X. We hasten to acknowledge, however, there remains an explicit physical and mathematical dependence on X. We present a graph of v_{unif} in Figure 4.

To determine u within the dissipative boundary layer we substitute (49) into (43), which can be written in the form

$$u_{\chi\chi} \;+\; 2\,\frac{\rho_\chi}{\rho}\,u_\chi \;=\; \gamma\,, \tag{52}$$

where

$$\rho(\chi) \;\equiv\; \sqrt{3}\,\mathrm{Ai}\big(\sqrt[3]{-\zeta_s u_s/2}\chi\big) \;+\; \mathrm{Bi}\big(\sqrt[3]{-\zeta_s u_s/2}\chi\big)\,.$$

Equation (52) can be integrated twice to yield

$$u \;=\; \gamma\int_0^\chi \frac{1}{\rho^2(\eta)}\int_0^\eta \rho^2(\theta)\,\mathrm{d}\theta\,\mathrm{d}\eta\,, \tag{53}$$

where we have imposed the smooth boundary conditions $u(0) = u_\chi(0) = 0$ (see (40)).

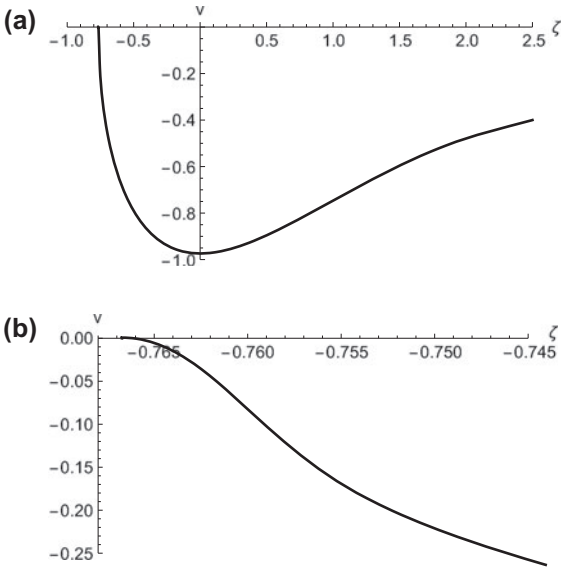

Figure 4. (a) Graph of v_{unif} vs. ζ along the $\mu = 0$ characteristic for $-0.77 \leq \zeta \leq 2.5$. (b) A blow up of (a) for the range $-0.77 \leq \zeta \leq -0.744$.

In summary, then, the leading order solution to (38), valid for $\zeta \to \zeta_s^+$ and $0 < R_E^{-1} \ll 1$, written in terms of the "outer" inviscid variables (within the inner equatorial region) ζ and u in (38), will be given by

$$u = u_s + \frac{\gamma}{R_E^{1/3}} \int_0^{R_E^{2/3}(\zeta-\zeta_s)} \frac{1}{\rho^2(\eta)} \int_0^{\eta} \rho^2(\theta)\, \mathrm{d}\theta\, \mathrm{d}\eta\,. \tag{54}$$

Again, it can be shown that the solution (54) asymptotically exactly matches, as $R_E \to \infty$, the inviscid "outer" solution (34).

Finally, the uniformly valid leading order solution for u, valid *both* in the "outer" inviscid and in the dissipation regions but within the inner equatorial region, will be given by

$$u_{\text{unif}} = u\big(\sigma(\zeta)\big) + \frac{\gamma}{R_E^{1/3}} \int_0^{R_E^{2/3}(\zeta-\zeta_s)} \frac{1}{\rho^2(\eta)} \int_0^{\eta} \rho^2(\theta)\, \mathrm{d}\theta\, \mathrm{d}\eta - \gamma\sqrt{-2(\zeta-\zeta_s)/(\zeta_s u_s)}\,, \tag{55}$$

where $u\big(\sigma(\zeta)\big)$ is determined by (23) and (24) with $\sigma\left(\zeta\right)$ the inverse function associated with $\zeta = \zeta\left(\sigma\right)$ where $\zeta\left(\sigma\right)$ is determined by (24), and where, again, we have suppressed the notational dependence on X.

Figure 4(a) is a graph of v_{unif} vs. ζ along the $\mu = 0$ characteristic for the range $-0.77 \simeq \zeta_s(0) \leq \zeta \leq \zeta_0 = 2.5$. Figure 4(a) is qualitatively very similar to the inviscid solution shown in Figure 3(b) except very near $\zeta \simeq \zeta_s^+$ (recall $R_E \simeq 2464$ for our scaling choices) where the boundary layer solution become dominant and smooths out the transition as $v \to 0$ as $\zeta \to \zeta_s^+$. Figure 4(b) is a "close-up" graph of v_{unif} vs. ζ along the $\mu = 0$ characteristic for the range $\zeta_s(0) \leq \zeta \leq -0.744$. Figure 4(b) shows the smooth transition as $\zeta \to \zeta_s^+$ in which $v \to 0$ and $v_\zeta \to 0$. A graph (not shown here) of the uniformly valid

solution u_{unif} shows an equally smooth transition as $\zeta \to \zeta_s^+$ in which $u \to u_s(0) \simeq 2.31$ and $u_\zeta \to 0$. The graphs for other characteristics curves are very similar.

3.3. The leading order height within the first dissipation region

With a bottom boundary layer present, the leading order (with respect to δ) mass equation in the inner equatorial region (see (16)) is given by

$$vuh_x + (vh)_\zeta = \widehat{r}\left(\nu^2 \partial_{xx} + \partial_{\zeta\zeta}\right)h, \tag{56}$$

where we have exploited the fact that u does not depend on x.

Our goal is to determine the structure of the leading order (bounded) solution to (56) within the dissipative region that asymptotically matches with the inviscid solution outside the dissipative region (but all within the inner equatorial region) given by (29). If the dissipation boundary layer variables (40) are substituted into (56), one obtains (after dropping the tildes)

$$\frac{v}{R_E^{1/3}}\left(u_s + u/R_E^{1/3}\right)h_x + (vh)_\chi = \frac{r\nu^2}{R_E^{4/3}}h_{xx} + rh_{\chi\chi}, \tag{57}$$

where it is assumed that $r \equiv R_E\widehat{r} \simeq \mathrm{O}(1)$, and where $v(\chi)$ will be given by (49).

To leading order in $R_E^{-1/3}$ (57) reduces to

$$rh_{\chi\chi} = (vh)_\chi, \tag{58}$$

which will be solved subject to the matching and boundary conditions

$$vh \to \frac{\gamma h_0\left(\widehat{\tau}\left(\mu(x,\zeta_s^+)\right)\right)}{\sin y_0} < 0 \qquad \text{as} \qquad \chi \to \infty, \tag{59}$$

$$h = 0 \qquad \text{for} \qquad \chi = 0, \tag{60}$$

respectively, where $\mu(x,\zeta_s^+)$ is the inverse mapping associated with the solution of the characteristic Equations (19) and (21). The matching condition (59) ensures that the meridional volume flux as one exits the dissipative boundary layer asymptotically matches the meridional volume flux in the inviscid region within the inner equatorial region (which is constant along the characteristics). The boundary condition (60) follows from the fact that the singularity in the velocity gradients in the inviscid solutions take place on the southern edge of the abyssal current where $v = 0$ in the trough of the stationary planetary wave. The "edge" of the abyssal current must correspond to a grounding or incropping in the height, i.e. must satisfy $h = 0$.

Equation (58) can be integrated once to yield

$$h_\chi - \frac{v(\chi)}{r}h = -\frac{1}{r}\Gamma(x),$$

$\Gamma\left(x\right)$ is a free integration constant. This equation can be integrated again to yield

$$h(x,\chi) \;=\; -\frac{1}{r}\Gamma(x)\int_0^{\chi}\exp\left[\frac{1}{r}\int_{\eta}^{\chi}\nu(\xi)\,\mathrm{d}\xi\right]\mathrm{d}\eta\,, \tag{61}$$

where $h(x,0) \;=\; 0$ has been imposed. To determine $\Gamma(x)$ we satisfy the matching condition (59).

The leading order behaviour of $h(x,\chi)$ as $\chi \;\to\; \infty$ can be determined as follows. Equation (61) can be re-written in the form

$$h(x,\chi) \;=\; \Gamma(x)\int_{t_0}^{0}\frac{\mathrm{e}^t}{\nu\big(\eta(t)\big)}\,\mathrm{d}t\,,$$

where the $(\eta \to t)$ substitution,

$$t \;=\; \frac{1}{r}\int_{\eta}^{\chi}\nu(\xi)\,\mathrm{d}\xi\,, \qquad\qquad t_0 \;\equiv\; \frac{1}{r}\int_{0}^{\chi}\nu(\xi)\,\mathrm{d}\xi\,,$$

has been used. Since

$$\varphi(z) \;\simeq\; -\sqrt{z} \qquad\quad \text{for} \qquad\quad z \gg 1\,,$$

(Abramowitz and Stegun 1970) it follows from (49) that

$$\nu \;\simeq\; -\sqrt[3]{-4\zeta_s u_s}\,\sqrt{\sqrt[3]{-\zeta_s u_s/2}\;\chi} \;=\; -\sqrt{-2\zeta_s u_s\,\chi} \to -\infty \qquad \text{as} \qquad \chi \to \infty\,,$$

which implies that $t_0 \to -\infty$ as $\chi \to \infty$. Thus, after an integration by parts, we obtain

$$h(x,\chi) \;\simeq\; \Gamma(x)\int_{-\infty}^{0}\frac{\mathrm{e}^t}{\nu\big(\eta(t)\big)}\,\mathrm{d}t \;\simeq\; \Gamma(x)\frac{\mathrm{e}^t}{\nu\big(\eta(t)\big)}\bigg|_{-\infty}^{0} + \text{h.o.t.} \;\simeq\; \frac{\Gamma(x)}{\nu(\chi)}\,,$$

since $t = 0 \Longrightarrow \eta = \chi$ (and where h.o.t. means "higher order terms"). Consequently, we conclude

$$h(x,\chi)\nu(\chi) \;=\; \Gamma(x) \qquad\quad \text{as} \qquad\quad \chi \to \infty\,,$$

which in order to satisfy (59) implies that

$$\Gamma(x) \;=\; \frac{\gamma h_0\big(\widehat{\tau}\big(\mu(x,\zeta_s^+)\big)\big)}{\sin y_0}\,. \tag{62}$$

In addition, this result clearly implies that $h_\chi \to 0$ as $\chi \to \infty$.

In summary, then, the leading order solution to (56), valid for $\zeta \;\simeq\; \zeta_s^+$ and $0 < \widehat{r} = rR_E^{-1} \;\ll\; 1$, written in terms of the "outer" inviscid variables (but all within the inner equatorial region) ζ and h in (56), will be given by

$$h \;=\; -\frac{1}{R_E^{2/3}\widehat{r}}\,\Gamma(x)\int_0^{R_E^{2/3}(\zeta-\zeta_s)}\exp\left[\frac{1}{R_E\widehat{r}}\int_{\eta}^{R_E^{2/3}(\zeta-\zeta_s)}\nu(\xi)\,\mathrm{d}\xi\right]\mathrm{d}\eta\,, \tag{63}$$

where $\nu\left(\xi\right)$ is given by (49) and $\Gamma\left(x\right)$ is given by (62). Again, within the context that $R_E\widehat{r} \;\simeq\; \mathrm{O}(1)$, it can be shown that the solution (63) asymptotically exactly matches, to

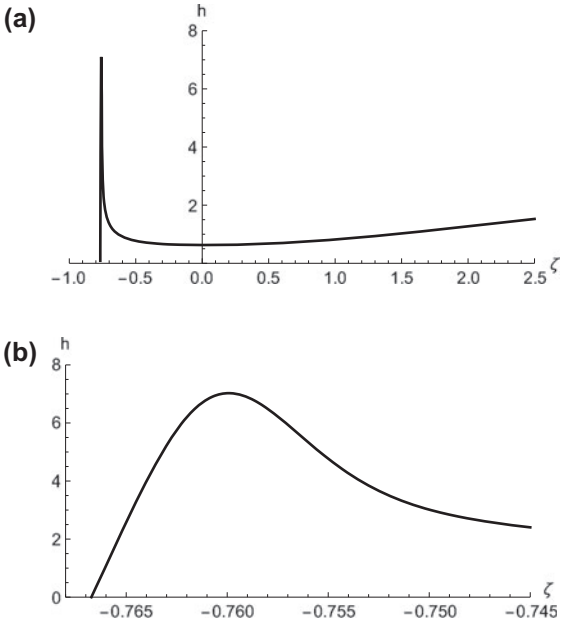

Figure 5. (a) Graph of h_{unif} vs. ζ along the $\mu = 0$ characteristic for $-0.77 \leq \zeta \leq 2.5$. (b) A blow up of (a) for the range $-0.77 \leq \zeta \leq -0.744$.

leading order as $R_E \to \infty$ (i.e. exiting the dissipation region) with the leading order "outer" solution (29) as it enters the dissipation region, i.e. $\zeta \to \zeta_s^+$.

Finally, the uniformly valid leading order solution for h, valid both in the "outer" inviscid and within the dissipation region, will be given by

$$h_{\text{unif}} = h(\mu,\sigma) + \frac{\gamma h_0\big(\widehat{\tau}\big(\mu(x,\zeta_s^+)\big)\big)}{\sin y_0\sqrt{-2\zeta_s u_s(\zeta-\zeta_s)}} - \frac{1}{R_E^{2/3}\widehat{r}}\,\Gamma(x)\int_0^{R_E^{2/3}(\zeta-\zeta_s)} \exp\left[\frac{1}{R_E\widehat{r}}\int_\eta^{R_E^{2/3}(\zeta-\zeta_s)} \nu(\xi)\,\mathrm{d}\xi\right]\mathrm{d}\eta\,, \tag{64}$$

where $h(\mu,\sigma)$ is determined by (29), with $\sigma(\zeta)$ and $\mu(x,\zeta)$ the inverse functions associated with $x(\mu,\sigma)$ and $\zeta(\sigma)$ determined by (25) and (24), respectively, and where we have suppressed the notational dependence on X.

Figure 5(a) is a graph of h_{unif} vs. ζ along the $\mu = 0$ characteristic for the range $-0.77 \simeq \zeta_s(0) \leq \zeta \leq \zeta_0 = 2.5$ (with $\widehat{r} = R_E^{-1} \Longrightarrow r = 1$). Figure 5(a) shows the initial decrease in h as ζ decreases from ζ_0 due to PV conservation in the intermediate region. As ζ enters the inner inviscid region h starts to increase as $|v|$ is decreasing in order to maintain meridional volume flux. Eventually dissipative processes dominate the dynamics and for $\zeta \simeq \zeta_s^+$ (recall $R_E \simeq 2464$ for our scaling choices) the boundary layer solution become dominant and $h \to 0$ as $\zeta \to \zeta_s^+$. Figure 5(b) is a "close-up" graph of h_{unif} vs. ζ along the $\mu = 0$ characteristic for the range $\zeta_s\,(0) \leq \zeta \leq -0.744$ showing the smooth transition as $\zeta \to \zeta_s^+$ in which $h \to 0$. Both figures also illustrate that the abyssal water "piles up" along the southern edge of the trough region in the stationary planetary wave ($|h_\zeta|$ significantly decreases as the dissipative boundary layer is exited). However, it is important to add that

the sharp peak for h_{unif} shown in Figure 5(a) could be considerably "spread out" over a larger range of ζ values if a larger value of the dissipation coefficient $\widehat{r}$ was assumed.

4. Conclusions

Oceanographic observations and high resolution numerical simulations using reduced models suggest (see the earlier references) that the kinematic flow properties of equator-crossing DWBCs (and for that matter the currents associated with deep water produced in Antarctica) are complicated. Much more complicated than the ability of present-generation ocean general circulation models (OGCMs) to accurately reproduce in anything other than crude bulk transport parameterisations. Indeed, it is not completely unreasonable to suggest that inter-hemispheric deep water exchange, required in the global convective overturning in the oceans, and critical to understanding climate variability over decadal and longer time scales, remains a significant area of uncertainty and is likely poorly parameterised in most present-generation OGCMs. Accordingly, it is vital that we develop a firm understanding of the basic geophysical fluid dynamic processes that act during the cross-equatorial flow of abyssal water masses. Not only with respect to improving our parameterisations of these processes for global-scale numerical models but also in suggesting further observational work that is required to more completely understand the detailed dynamics of these currents in the equatorial region.

Theoretical and numerical modelling, and observations suggest that these abyssal flows conserve, to leading order, planetary geostrophic PV in midlatitudes. Since the sign of the Coriolis parameter changes across the equator this means that additional dynamics, particularly dissipation, becomes important in the cross-equatorial dynamics. Numerical and theoretical modelling suggests that the dissipation zones correspond to "relatively small" isolated zonally-elongated regions that are located in the trough and crest associated with a nonlinear stationary planetary wave that is formed by these abyssal flows as they flow zonally across the Atlantic Ocean along the equator (this wave is seen in the oceanographic observations).

Building upon earlier theoretical work that describes the large scale inviscid structure of the DWBCs as flow from midlatitudes into the equatorial region and cross the equator, we have advanced a simple but informative nonlinear dissipative theory to model the regularisation of the abyssal flow as it enters the first dissipative region (which corresponds to a region of intersecting characteristics in the large scale inviscid flow) located in the trough of the stationary planetary wave. Although other choices are possible, we have focused on the role that could be played by horizontal mixing in the momentum equations and by bottom friction (or possibly entrainment between the abyssal water mass and the overlying ocean) in the mass conservation equation. Indeed, further observational work is needed to specify precisely what are the dominant dissipative processes occurring in the equatorial region associated with these currents. For the nonlinear dissipation model presented here, it was possible to obtain an explicit leading order solution in the dissipative region that smoothly satisfies the appropriate boundary conditions and smoothly matches asymptotically with the large scale inviscid flow structure outside the dissipation zones.

Although there is considerable uncertainty in the value of the dissipation parameters (again further observational work is needed here) we find a horizontal dissipation length scale of about 1.2 km with the dissipation occurring in a zonal region that is about 10

km wide meridionally and about 150 km long zonally, and that is located in the trough (and the crest region – but not examined here) of the stationary planetary wave, which we suggest would be located about 170 km south of the equator about 400 km east of where the DWBC first crosses the equator. Our modelling suggests that the dissipation is strongly localised along the southern edge, grounding or incropping of these grounded abyssal currents. Again, these are highly speculative estimates, but hopefully they suggest a starting point for further research.

Disclosure statement

No potential conflict of interest was reported by the author.

Funding

This work was partially supported by Discovery Research Grants awarded by the Natural Sciences and Engineering Research Council [NSERC RGPIN 05038].

References

Abramowitz, M. and Stegun, I.A., 1970. *Handbook of mathematical functions*. 9th ed. New York: Dover.

Baehr, J., *et al.*, 2009. Observed and simulated estimates of the meridional overturning circulation at 26.5N in the Atlantic. *Ocean Science*, 5, 575–589.

Bender, C.M. and Orszag, S.A., 1978. *Advanced mathematical methods for scientists and engineers*. New York: McGraw-Hill.

Borisov, S. and Nof, D., 1998. Deep, cross-equatorial eddies. *Geophysical & Astrophysical Fluid Dynamics*, 87, 273–310.

Choboter, P.F. and Swaters, G.E., 2004. Shallow water modeling of Antarctic Bottom Water crossing the equator. *Journal of Geophysical Research*, 109, C03038.

Cunningham, S.A., *et al.*, 2007. Temporal variability of the Atlantic meridional overturning circulation at 26.5N. *Science*, 317, 935–938.

Cushman-Roisin, B., 1982. Motion of a free particle on a beta-plane. *Geophysical & Astrophysical Fluid Dynamics*, 22, 85–102.

Dengler, M., *et al.*, 2004. Break-up of the Atlantic deep western boundary current into eddies at 8° S. *Nature*, 432, 1018–1020.

Edwards, C.A. and Pedlosky, J., 1998a. Dynamics of nonlinear cross-equatorial flow. Part I: potential vorticity transformation. *Journal of Physical Oceanography*, 28, 2382–2406.

Edwards, C.A. and Pedlosky, J., 1998b. Dynamics of nonlinear cross-equatorial flow. Part II: the tropically enhanced instability of the western boundary current. *Journal of Physical Oceanography*, 28, 2407–2417.

Fischer, J. and Schott, F.A., 1997. Seasonal transport variability of the deep western boundary current in the equatorial Atlantic. *Journal of Geophysical Research*, 102, 27751–27769.

Gouriou, Y., *et al.*, 2001. Deep circulation in the equatorial Atlantic ocean. *Geophysical Research Letters*, 28, 819–822.

Joyce, T.M., *et al.*, 2005. On the deep western boundary current south of Cape Cod. *Deep-sea Research*, 52, 615–625.

Kim, A., Swaters, G.E., and Sutherland, B.R., 2014. Cross-equatorial flow of grounded abyssal ocean currents. *Geophysical & Astrophysical Fluid Dynamics*, 108, 363–386.

McCartney, M.S., 1993. Crossing of the equator by the deep western boundary current in the western Atlantic Ocean. *Journal of Physical Oceanography*, 23, 1953–1974.

McCartney, M.S. and Curry, R.A., 1993. Transequatorial flow of Antarctic Bottom Water in the western Atlantic Ocean: abyssal geostrophy at the equator. *Journal of Physical Oceanography*, 23, 1264–1276.

Nof, D., 1983. The translation of isolated cold eddies on a sloping bottom. *Deep-sea Research*, 30, 171–182.

Nof, D. and Borisov, S., 1998. Inter-hemispheric oceanic exchange. *Quarterly Journal of the Royal Meteorological Society*, 124, 2829–2866.

Pedlosky, J., 1987. *Geophysical fluid dynamics*. New York: Springer.

Philander, S.G.H., 1971. The equatorial dynamics of a shallow, homogeneous ocean. *Geophysical & Astrophysical Fluid Dynamics*, 2, 219–245.

Richardson, P.L. and Fratantoni, D.M., 1999. Float trajectories in the deep western boundary current and deep equatorial jets of the tropical Atlantic. *Deep Sea Research Part II: Topical Studies in Oceanography*, 46, 305–333.

Spall, M.A., 1994. Wave-induced abyssal recirculations. *Journal of Marine Research*, 52, 1051–1080.

Swaters, G.E., 2013. Flow of grounded abyssal ocean currents along zonally-varying topography on a rotating sphere. *Geophysical & Astrophysical Fluid Dynamics*, 107, 564–586.

Swaters, G.E., 2015a. Midlatitude-equatorial dynamics of a grounded deep western boundary current. Part I. Midlatitude flow and the transition to the equatorial region. *Journal of Physical Oceanography*, 45, 2457–2469.

Swaters, G.E., 2015b. Midlatitude-equatorial dynamics of a grounded deep western boundary current. Part II. Cross-equatorial dynamics. *Journal of Physical Oceanography*, 45, 2470–2483.

Thierry, V., Mercier, H., and Treguier, A.M., 1998. Direct observations of low frequency fluctuations in the deep equatorial Atlantic. *Annales Geophysicae II: Hydrology, Oceans and Atmospheres*, 16 (Suppl. 11), C568.

Toole, J.M., *et al.*, 2011. Transport of the North Atlantic deep western boundary current about 39°N, 70°W: 2004—2008. *Deep Sea Research Part II: Topical Studies in Oceanography*, 58, 1768–1780.